Computer-aided recognition of a four-chamber image plane in three-dimensional echocardiographic images of children

Xiaoping Liu,[a] Xin Yang,[a] Lanping Wu,[b] Kun Sun,[b] Yanfeng Shang,[a,c] and Rudi Deklerck[c]
[a]Shanghai Jiaotong University, Institute of Image Processing and Pattern Recognition, Shanghai, China
[b]Shanghai Jiaotong University, Shanghai Children's Medical Center, Shanghai, China
[c]Vrije Universiteit Brussel, Department of Electronics and Informatics, Interdisciplinair Instituut voor BreedBand Technologie, 1050 Brussel, Belgium
E-mail: Lxp_0710@sjtu.edu.cn

Abstract. *Automated detection of the clinically relevant image planes in a three-dimensional echocardiographic (3-DE) data set has potential applications for diagnosis of pediatric congenital heart disease. We propose a method based on template matching to automatically detect the four-chamber image plane (4CIP) in a 3-DE data set. First, a normal four-chamber image is chosen as the template. Second, to find the 4CIP in a 3-D volume, a series of cross sections are extracted from this volume. Then, a coarse-to-fine retrieval is applied to the stack of slices and the image most similar to the template is proposed as the 4CIP of this volume. We tested the method on 28 data sets of normal children and 22 data sets of children suffering from congenital heart disease, and the error rates are 7 and 9%, respectively. As will be shown, the autodetection algorithm can be straightforwardly implemented, has low computational complexity, and is robust to noise. © 2008 SPIE and IS&T.* [DOI: 10.1117/1.2956009]

1 Introduction

During the retrospective review of three-dimensional echocardiographic (3-DE) data sets for diagnosis and analysis of pediatric congenital heart disease (CHD), it takes time for the medical doctor to find the clinically relevant image planes. 3-DE images are usually acquired from the parasternal, subcostal, and apical windows, but for assessment of atrioventricular septal defects, heart valve diseases, etc., the apical data sets are, in general, preferred for making the diagnosis. Among several clinically relevant image planes, the four-chamber image plane (4CIP) is the most important one. Consequently, as a preliminary study, this paper focuses on the automated detection of the 4CIP in apical data sets. This autodetection will be a useful tool for the medical doctors during retrospective review. Furthermore, it can be a prior procedure for image registration, i.e., for merging 3-DE images with images of different modalities.

The 4CIP in a 3-DE data set can be detected by aligning the volumetric data with a 3-D template image in which the 4CIP has been previously identified. However, the computational complexity for 3-DE image registration[1,2] is high, and it is troublesome to register 3-DE images of different subjects. In order to automatically recognize the 4C image, Matthew *et al.* used peak features,[3] which is useful in the case of the ideal condition when the whole heart is visible and located in the middle of the image. Another group presented a method based on template matching by elastic registration,[4] which can still work very well when only part of the heart is visible and the location of the heart is not in the middle. However, as a 3-D data set may contain hundreds of 2-D images, it is time-consuming to match the four-chamber (4C) image in a 3-D volume by elastic registration. In our research, we developed a fast automatic method to find the 4CIP in the 3-DE images, suitable for the real-time applications, where first, a typical end-diastolic 4C image is chosen as a template. Second, in order to find the 4CIP in a 3-D data set, an image database is built by extracting cross sections from the end-diastolic volume of the data set. Then by a coarse-to-fine search, the most similar image of the template is retrieved from the stack of images as the 4CIP of the data set.

2 Methods

2.1 *Template Selection*

As illustrated in Fig. 1, an end-diastolic 4C image of a normal child is selected and a rectangular region located at the center of the image is chosen as a template. The distribution of the septum and chambers in the rectangular region of the end-diastolic 4C image is considerably different from that of the other image planes and is weakly affected by the variation of the heart size, shape, and the image intensities. Therefore, it can easily detect the most similar images without requiring a huge template library.

2.2 *Image Database Construction*

To detect the 4CIP in a 3-DE data set, an image database including cross sections extracted from the end-diastolic volume of the data set is built. Here, the echocardiographic volume is like a truncated pyramid. As shown in Fig. 2, we assume that the cardiac apex is the vertex of the pyramid, which is chosen as the origin O, and that the long axis of

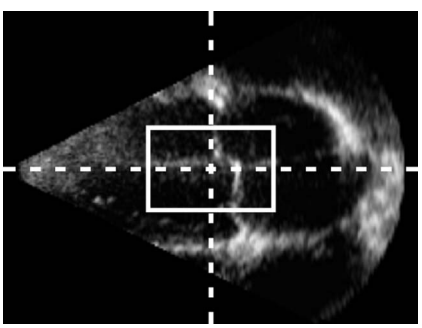

Fig. 1 Rectangular region defined in the apical 4C image.

Paper 07183LRR received Feb. 9, 2008; revised manuscript received Apr. 18, 2008; accepted for publication May 2, 2008; published online Jul. 15, 2008.

1017-9909/2008/17(3)/030502/3/$25.00 © 2008 SPIE and IS&T.

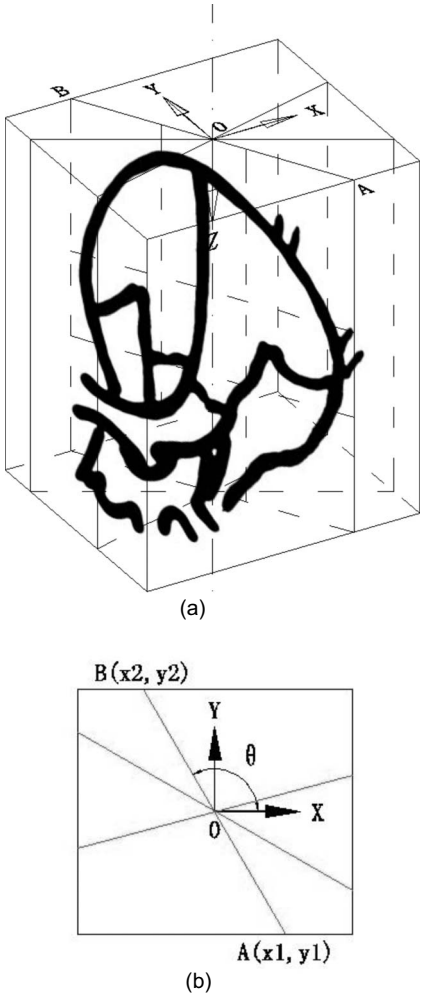

Fig. 2 Coordinate system of the apical volumetric data set: (a) 3-D distribution of the cross sections and (b) Projection of the cross sections in the XOY plane.

the heart passing through the apex is the vertical axis OZ. The 4CIP is recognized among the cross sections sharing a common symmetric axis OZ. The projection of each cross section in the XOY plane is a radial line like AB. A point P is located on the cross section if its coordinates satisfy the following:

$$\begin{cases} x = x1 + l\cos\theta \\ y = y1 + l\sin\theta \end{cases}, \quad (0 \leqslant \theta < 180 \text{ deg}), \tag{1}$$

where θ is the angle between line AB and the positive axis OX as shown in Fig. 2(b), ranging from 0 to 180 deg, and l is the Euclidean distance from the projective point of P in the XOY plane to point A, ranging from 1 to L, which is the length of each cross section, defined as follows:

$$L = \overline{AB} = \sqrt{(x2 - x1)^2 + (y2 - y1)^2}. \tag{2}$$

Each cross section's size is $L \times n$ pixels, where n is the volume's size in the OZ direction. The units of the sizes in this paper are pixels.

2.3 *Four-Chamber Image Retrieval*

To improve the speed and accuracy of the 4C image retrieval, a coarse-to-fine strategy is utilized. First, the coarse retrieval is performed by comparing the cumulative histograms[5] of the two images. Because of transducer movement artifacts and the respiration of the patient, the centered cross-shaped septum may shift away from the image center by 10–20 pixels. Because the image histogram is rather invariant to an affine transformation, it is quite robust for the generally occurring misalignments. The cumulative histogram is implemented in the rectangular region shown in Fig. 1, whose geometric center is the same as that of each cross section. By the coarse retrieval, the first 60 most similar images are selected from the original 180 images for each data set.

Next, to further cope with the misalignment error, a rigid registration approach is adopted to find the best match of the rectangular region in each image of the reduced image set, resulting from the coarse retrieval based on similarity in the cumulative histograms. For the rigid registration, we selected the cross-correlation as the similarity measure and the simplex optimization method to find the optimized scale, translation, and rotation parameters. The images selected by the coarse retrieval procedure are then each aligned to the template image according to their optimal transformation parameters. In this way, geometrical transformation influences on the wavelet features computed in the fine retrieval procedure will be strongly reduced.

Finally, because the rectangular region in the middle of a 4C image contains distinct edges, we selected the high-frequency details of the image as the feature for the fine retrieval. The wavelet domain yields a multiresolution decomposition so that high-frequency information can be extracted from the high-frequency subbands. The original image constrained to the rectangular region is decomposed into four subbands, LL1, HL1, HV1, and HD1, by means of the db2 wavelet. The mean E and the variance V of the wavelet coefficients of the three high-frequency subbands, HL1, HV1, and HD1, are selected as the features. E and V are defined by

$$E = \frac{1}{MN}\sum_{m=1}^{M}\sum_{n=1}^{N}|x(m,n)| \tag{3}$$

$$\text{and } V = \frac{1}{MN}\sum_{m=1}^{M}\sum_{n=1}^{N}|x(m,n)^2 - E^2|, \tag{4}$$

where M and N are the dimensions of the high-frequency subband S; $x(m,n)$ are its corresponding wavelet coefficients; and $S \in \{\text{HL1}, \text{HV1}, \text{HD1}\}$. The Euclidean distance of the feature vectors, $(\mathbf{E}_{\text{HL1}}, \mathbf{V}_{\text{HL1}}, \mathbf{E}_{\text{HV1}}, \mathbf{V}_{\text{HV1}}, \mathbf{E}_{\text{HD1}}, \mathbf{V}_{\text{HD1}})$, of two images is employed to measure the image dissimilarity. In the end, the cross-section image with minimum dissimilarity is retrieved as the 4C image from the images left after the coarse selection.

3 Experimental Results

The data used in this study were full-volume data acquired with Philips Sonos7500 US equipment and comprised 28 data sets of 16 normal subjects aged from

Table 1 Medical data of the subjects for whom the 4C images are shown in Fig. 3 (LVDD: left ventricular end diastolic dimension; LVEF: left ventricular ejection fraction).

Figure No.	Study Subjects	Gender	Age	LVDD (cm)	LVEF (%)
3(a)	normal	male	1 month	2.74	66
3(b)	normal	male	5 yr	3.50	73
3(c)	normal	female	12 yr	4.30	64
3(d)	CAVC	male	3 months	2.18	74
3(e)	CAVC	female	5 yr	2.95	71
3(f)	CAVC	male	13 yr	3.77	57

1 month to 12 years and 22 data sets of 14 patients with common atrioventricular canal (CAVC), aged from 3 months to 13 years. The total calculation time is <20 s for each data set on a PC with a 2.4 GHz Pentium 4 processor. Figure 3 shows the 4C images detected in the datasets of six subjects by our method. The medical data of these subjects are listed in Table 1.

To evaluate our method quantitatively, we use θ, as shown in Fig. 2, to denote the angle of direction of the 4CIP. The image plane showing four chambers (i.e., the left and right atria and ventricles, two large atrioventricular valves, the interventricular septum, and interatrial septum) is an acceptable 4CIP, while an image plane containing the aortic valve is not considered to be a 4CIP. Three experienced sonographers were asked to manually search the 4CIP for each data set. However, because the shape of the heart changes continuously, it is impossible for the medical doctors to define a unique 4CIP in the data set, but rather a range of angles has to be considered as valid 4C image planes. The plane in the center of this range is then accepted as the reference 4CIP. In order to determine a reasonable range for the acceptable 4CIP, a 4CIP lib, which includes cross sections from all data sets with e, the absolute deviation angle from the reference 4CIP, ranging from 0 to 20 deg, was tested by the echocardiographers. Finally, $e \leqslant 10$ deg is selected as the reliable range of the acceptable

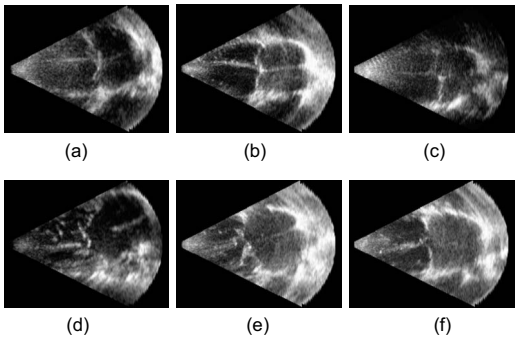

Fig. 3 4C images automatically detected by our method in six data sets of three normal children and three children suffering from CAVC.

Table 2 List of the error rates with different e.

e	Error Rates of Normal Data Sets (%)	Error Rates of Abnormal Data Sets (%)
0–3	32	36
3–6	25	18
6–8	7	14
8–10	7	9
>10	4	9

4CIP because the doctors accepted the 4CIP in this range with more than 99% confidence. We computed the cumulative frequency table (see Table 2) in terms of the absolute deviation angle e, calculated for each of the 4C images found automatically via our coarse-to-fine retrieval method. Considering $e \leqslant 10$ deg as the range of acceptance, the error rates of our method are 7% for the 28 studies of the normal children and 9% for 22 studies of the children suffering from CAVC, respectively. When realizing tests with other templates, we observed that the template with high echo quality, in particular, with highly visible ventricular walls, performed best because less noise could affect the result.

4 Conclusions

With low computational complexity and a simple implementation, our method can automatically find the 4CIP in the apical data sets of different subjects by using only one 4C template image of a normal subject. With the detected 4CIP, it is easier to find the short-axis and long-axis image planes in the data sets. At this moment, we only tried the 4CIP detection in apical data sets of children, but because the variability of the heart is smaller among adults than among children, we do not expect too many problems when applying the autodetection scheme on cardiac images of adults. Furthermore, it remains worthwhile to detect clinically relevant image planes in parasternal and subcostal data sets, but for these data sets the current approach may need to be adapted.

References

1. R. Shekhar and V. Zagrodsky, "Mutual information-based rigid and non-rigid registration of ultrasound volumes," *IEEE Trans. Med. Imaging* **21**(1), 9–22 (2002).
2. R. Shekhar, V. Zagrodsky, M. J. Garcia, and J. D. Thomas, "Registration of real-time 3-D ultrasound images of the heart for novel 3-D stress echocardiography," *IEEE Trans. Med. Imaging* **23**(9), 1141–1149 (2004).
3. E. O. Matthew, B. Jinbo, K. Sriram, R. Bharat, S. Jonathan, K. Alan, H. Jing, and P. Srinivasan, "Automatic view recognition for cardiac ultrasound images," in *Proc. 1st MICCAI'06-CVII*, pp. 187–194 (2006).
4. S. V. Aschkenasy, C. Jansen, R. Osterwalder, A. Linka, M. Unser, S. Marsch, and P. Hunziker, "Unsupervised image classification of medical ultrasound data by multiresolution elastic registration," *Ultrasound Med. Biol.* **32**(7), 1047–1054 (2006).
5. M. Stricker and M. Orengo, "Similarity of Color Images," *Proc. SPIE* **2420**, 381–392 (1995).